Numerical investigation of "Detachment cone" in the magnetic nozzle

IEPC-2019-324

Presented at the 36th International Electric Propulsion Conference
University of Vienna • Vienna, Austria
September 15-20, 2019

Z.Y. Chen[1], Y. B. Wang[2], J. X. Ren[3], P. Wu[4]
School of Astronautics, Beihang University, Beijing, 100083, China

M. Li[5]
Innovation Academy for Microsatellites of CAS, Shanghai, 201203, China

H. B. Tang[6]
School of Space and Environment, Beihang University, Beijing, 100083, China

Abstract: Magnetic nozzles (MN) are convergent-divergent applied magnetic fields commonly used to guide, expand and accelerate plasma. In electric propulsion, MNs are used to enhance the propulsive performance of plasma thrusters like VASIMR, AF-MPDT, helicon thrusters etc. In the experiment of the 15kW AF-MPDT at Joint Laboratory of Plasma and Propulsion, a dark-colored cone region named "Detachment Cone" is observed in the plume which separate the plume into two parts – the central main beam and the side beam. Similar distribution of plasma density is obtained through a single Langmuir probe in the experiment, which confirms the existence of the cone structure. In order to investigate the mechanism of this phenomenon, a 2D3V Particle-in-Cell model is used to simulate the magnetic nozzle. The detachment cone is reproduced in the simulation. It is believed that the cause of the detachment cone is that the thermalized ions injected from the plasma inlet expands out of the maximum diverging magnetic field lines (MDMFL) due to insufficient magnetization. And a parametric study on the influence of magnetic inductive strength and ion temperature is conducted to investigate the phenomenon. Strengthening the magnetic field can effectively suppress the phenomenon by two competing mechanisms – ion magnetization and the potential barrier. And depositing more energy into electrons than ions can help suppress the detachment cone.

Nomenclature

m_i	=	mass of the ion
m_e	=	mass of the electron
λ_{d0}	=	Debye length at the plasma inlet
R_{p0}	=	radius of the plasma inlet
$f(v_{ex})$	=	distribution function of the *X* component of electron thermal velocity
$f(v_{ey})$	=	distribution function of the *Y* component of electron thermal velocity

[1] PhD Candidate, Department of Propulsion, School of Astronautics, chenzhiyuan@buaa.edu.cn.
[2] Associate Professor, Department of Propulsion, School of Astronautics, wangyibai@buaa.edu.cn
[3] Associate Professor, Department of Propulsion, School of Astronautics, rjx_buaa@163.com
[4] PhD Candidate, Department of Propulsion, School of Astronautics, 13151149@buaa.edu.cn.
[5] Research fellow, Institute of Satellite Control Technology, limin_buaa@me.com.
[6] Professor, Department of Space Science, School of Space and Environment, thb@buaa.edu.cn.

$f(v_{ez})$	=	distribution function of the *Z* component of electron thermal velocity
$f(v_{ix})$	=	distribution function of the *X* component of ion thermal velocity
$f(v_{iy})$	=	distribution function of the *Y* component of ion thermal velocity
$f(v_{iz})$	=	distribution function of the *Z* component of ion thermal velocity
k_B	=	Boltzmann constant
T_{e0}	=	electron temperature at the plasma inlet
T_{i0}	=	ion temperature at the plasma inlet
v_{ex}	=	*X* component of electron thermal velocity
v_{ey}	=	*Y* component of electron thermal velocity
v_{ez}	=	*Z* component of electron thermal velocity
v_{ix}	=	*X* component of ion thermal velocity
v_{iy}	=	*Y* component of ion thermal velocity
v_{iz}	=	*Z* component of ion thermal velocity
v_0	=	drifting velocity of ions at the plasma inlet
Ω_{i0}	=	ion cyclone frequency at the plasma inlet
B_0	=	magnetic inductive strength at the plasma inlet
r_{Li}	=	ion Larmor radius at the plasma inlet
r_{Le}	=	electron Larmor radius at the plasma inlet
q_i	=	charge of the ions
q_e	=	charge of the electrons
$\hat{z}$	=	normalized z coordinates

I.Introduction

Magnetic nozzles are usually convergent-divergent magnetic field used to guide the plasma flow and transfer the non-directed kinetic energy to the directed one. They are commonly used in electric propulsion[1–4], advanced manufacturing and material processing[5]. The magnetic nozzle acts functionally like a de Laval nozzle, but incorporates plasma-field interactions to constrain and accelerate the plasma flow, which avoids direct wall-plasma contact that may damage the wall in the long run. Moreover, the shape of the magnetic nozzle can be easily changed to control the thrust vector without using the mechanical gimbals[6–8].

Ever since the concept of magnetic nozzles is put forward, numerous studies have been done to explore the physics in MNs, either by experiments[9–12] or numerical simulations[13–18]. These pioneer studies gained much insights into the physical details of magnetic nozzles and revealed the existence of ambipolar acceleration. In recent years, Arefiev et al. developed the rarefication wave theory[19] and Sheehan et al. presented the adiabatic expansion theory[20] to further explain the ambipolar acceleration. What's more, another acceleration mechanism featuring a potential structure named current-free double layer has been reported to exist in the MN of helicon plasma thrusters (HPTs)[2]. In recent 25 years, many of the research interests had moved to detachment processes in MNs. Based on different cold MHD models, Moses et al.[21], Hooper[22] and Arefiev and Breizman[23] put forward different detachment mechanisms related to resistivity, electron inertia and induced magnetic field respectively. The inertia detachment has been studied extensively, some believe the hybrid Larmor radius can be an effective criterion for detachment[22,24,25] while others argue that only electron demagnetization guarantees detachment[26]. About the induced field detachment, Ilin et al.[27] and Winglee et al.[28] acquired similar conclusions to that of Arefiev and Breizman[23]. Whereas, the direction of induced current is much debated, and the self-demagnetization detachment has been proposed[29,30]. Detachment may also be achieved through recombination[31], charge exchange collisions and magnetic reconnection.

In the recent magnetoplasmadynamic thruster (MPDT) magnetic nozzle experiment conducted at the Joint Laboratory of Plasma and Propulsion (JLPP) of Beihang University, a strange plume structure was observed as shown in Fig.1 -- A dark-colored cone region is observed in the plume which separate the plume into two parts – the collimated central plume and the periphery part. This phenomenon is named as "the detachment cone" as it's related to the particle detachment from the magnetic field, and it has been reported by our group[32] in IEPC 2013 but not investigated in detail. The plasma density is obtained using an Langmuir single probe which demonstrates the detachment cone clearly as shown in Fig 2.

Other than the paper of Xu et al.[32], there exists no public report plume structures like the detachment cone. Some other plume structures that associates with hollow area of plasma density have been discovered and investigated in the magnetic nozzle, such as the high density conic[33] and the self-collimation[28]. These two phenomena are both observed in the magnetic nozzle of helicon thrusters.

The high density conic was first discovered by C. Charles[33], the high density conic is a U-shaped conic area that forms in the direct downstream of the plasma inlet of the magnetic nozzle of helicon thruster, where the plasma density is about 30% higher than surrounding regions. This is related to the detachment cone because the outer part of the detachment cone is a high density conic resembles the high density conic. This phenomenon is later explained by Takahashi et al.[34] that a bi-Maxwellian population of electrons with a hot tail at 9eV travelling downstream along the "most divergent magnetic line" increases the ionization rate along the way and is responsible for the high density in the conic area. However, there's another explanation put forward by Saha et al.[35] that the ions are trapped near the conical surface by the electric potential well generated by the ions' overshoot driven by the radial component of double layer[36,37]. And there is no evidence of bi-Maxwellian electrons found in the experiment taken by Saha et al[35], contradicting to Charles' diagnostic results.

The self-collimation is a phenomenon that the beam radius become smaller instead of larger downstream discovered by Winglee et al. through experiment and MHD simulation of magnetic nozzle in the helicon thruster[28]. It is related because it resembles the inner collimated part of the plume in the center of detachment cone. Winglee et al. claimed that the self-collimation is due to the frozen-in theorem where the super-Alfvénic plasma plume will pull the magnetic field along with it. The perturbed magnetic field induced by the paramagnetic plasma currents changed the topology of magnetic field and make the magnetic lines flatter. However, this simulation is conducted under the assumption that the plasma is cold, thus unpractical for propulsion purposes and unfit for the situation we observed in the MPDT plume.

To clarify the physical insights of this phenomenon, a 2D3V particle-in-cell code is employed to investigate it. It is discovered that the Lorenz force generated from the interaction between the induced plasma currents and the applied magnetic field is the main cause of this unusual plume structure. The rest of this paper is arranged as follows, part two introduces the PIC method and boundary conditions of the model, part three presents the reproduction of the detachment cone by computation, analyzes the causes of phenomenon, and discusses the influence of ion temperature and magnetic inductive strength on the it. And part four concludes the paper.

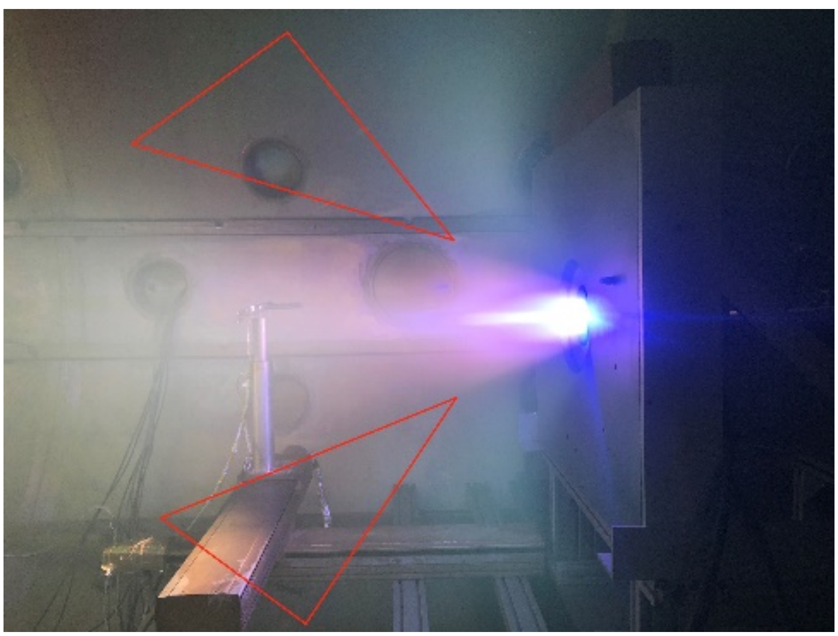

Figure 1 The detachment cone observed in the MPDT experiment at JLPP.

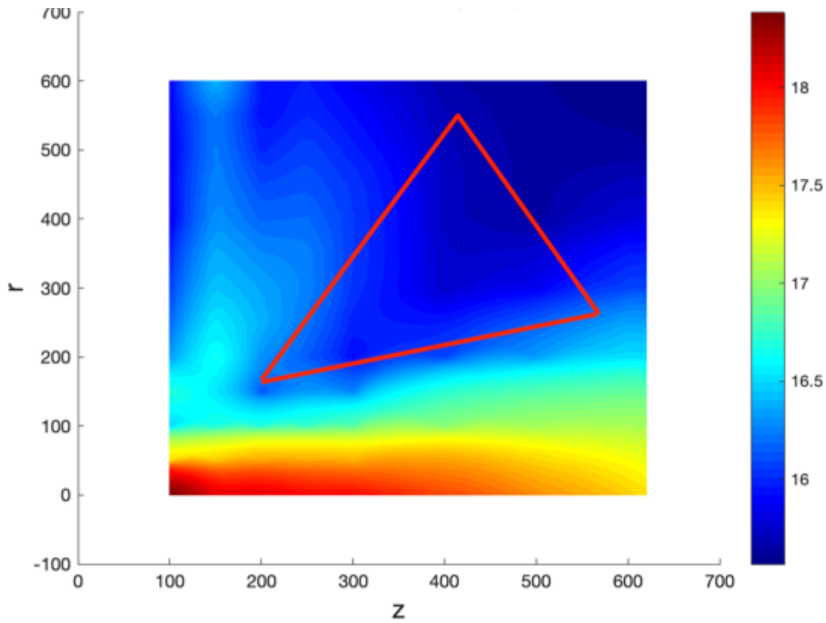

Figure 2 Electron number density contour measured in the AF-MPDT experiment at JLPP. (the legend in logarithmic units)

II. Methodology

A. General introduction of the numerical methods

As the ion temperature in the MPDT and VASIMR cannot be safely neglected, our PIC model should include the warm ion effect in the plasma inlet. To include this effect, the fully kinetic planar-3V PIC model reported in our previous work [36] is extended to include warm-ion inlet and background magnetic field, which is then used to simulate the magnetic nozzle with a nonuniform inlet in this paper.

In this case, the plasma is assumed to be fully ionized and collisionless as the mean free path is orders of magnitude larger than the size of magnetic nozzle throat, which is usually used as a characteristic length in the MN studies[38]. The computational domain is depicted as in Fig 3. The magnetic field used in the code is generated by the same magnetic coil that supplied the applied field of the AF-MPDT and measured with a Gauss meter then import into the program.

In the PIC model, ions and electrons are modeled as macro particles separately. And macro particles are moved by solving Newton-Lorentz equations using Boris scheme. And the self-consistent electric field is calculated by solving Poisson equations with DADI method. For the program, the induced magnetic field can also be calculated consistently by solving the magnetic vector potential using the same DADI solver and a larger computational domain, however this function is disabled due to the small value of the induced field compared to the applied one (3 orders smaller as we obtained in the computation test).

Because of the uncertainty of the effects on the simulation results brought by the acceleration methods of PIC, these methods are not incorporated into the code, instead, the simulation domain is shrunken to a few hundred Debye lengths and the real mass ratio of proton to electron $m_i/m_e = 1836$ is used, so that the computational cost can be effectively cut down.

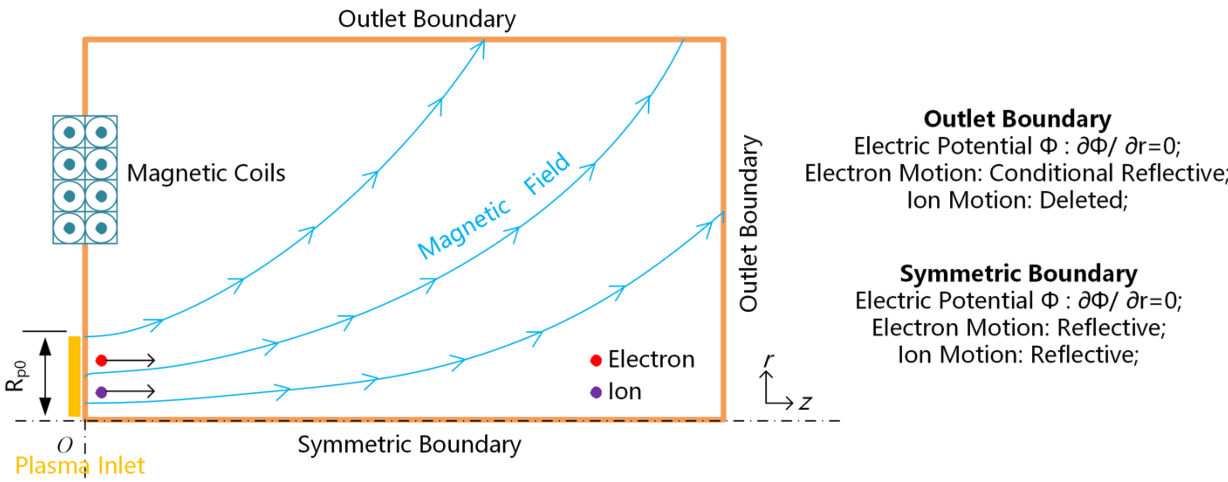

Figure 3 computational domain and boundary conditions

As depicted in Figure 3, the computational domain is a rectangle area and the Debye length at the entrance λ_{D0} is taken as the cell size. The domian has the length of $200\lambda_{D0}$ and a width of $120\lambda_{D0}$. The lower part of the left boundary stands for the plasma inlet (particle emission plane) with a length of $R_{p0} = 10\ \lambda_{D0}$. The boundary on the bottom is the symmetric boundary. Other boundaries (left up, up and right) are open boundaries representing the vacuum environment. The central plane of the magnetic coil coincides with the plane represented by the left boundary, the center of the coil is at the origin, which means the plasma inlet is also the magnetic nozzle throat.

B. Boundary conditions

Since the induced magnetic field is neglected, there remains only two kind of boundary conditions: electric field and particle movements. For electric field boundary, the potential of original point is set to 0V as a reference potential and the potential profile in the plasma inlet is determined by the Boltzmann relation.

The open boundaries and the symmetric boundary are set as Neumann condition. The particle motion boundary conditions are much more complicated than those of electric field.

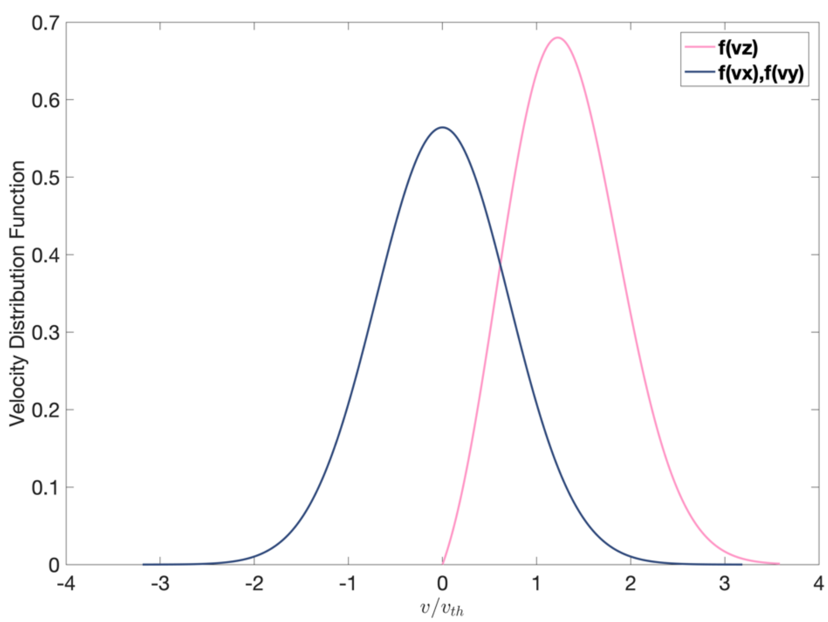

Figure 4 Particle velocity distribution functions at plasma inlet

At each time step, ions and electrons are emitted from the inlet boundary along the z axis, the Mach number of the inlet plasma is 1.0, and the density profile is assumed to be uniform. The electrons are sampled from a Maxwellian distribution with a drift component equals to the ion drifting velocity. Since the ion temperature is not negligible in the current model, and the ions have a drift velocity v_0 corresponding to Mach=1, the ion velocity distribution in the z direction needs to use the drifting Maxwellian flux distribution, and the other directions still follow a stationary Maxwellian distribution[39]. The velocity distribution function of electrons and ions are as follows,

$$f_e(v_{ex,ey,ez}) = \sqrt{\frac{m_e}{2\pi k_b T_{e0}}} exp\left(-\frac{m_e}{2k_b T_{e0}} v_{ex,ey,ez}^2\right) \tag{1}$$

$$f_i(v_{ix,iy}) = \sqrt{\frac{m_i}{2\pi k_b T_{i0}}} exp\left(-\frac{m_i}{2k_b T_{i0}} v_{ix,iy}^2\right) \tag{2}$$

$$f_i(v_{iz}) = A\, v_{iz}\; exp\left(-\frac{m_i}{2k_b T_{i0}} (v_{iz} - v_0)^2\right) \tag{3}$$

The coefficient A in equation (3) can be obtained through normalization conditions.

$$A^{-1} = \sqrt{\frac{k_b T_i}{2\pi m_i}} \cdot \exp\left(-\frac{m v_0^2}{2k_b T_i}\right) + \frac{v_0}{2}\left(\mathrm{erf}\left(v_0 \cdot \sqrt{\frac{m_i}{2k_b T_i}}\right) + 1\right) \tag{4}$$

The velocity distribution function of ions is illustrated in Figure 4.

As stated in our previous work[40,41], we think quasi-neutrality and current-free condition should both be conserved globally within the plasma source. However, considering the counter streaming of electrons[19], it is difficult to guarantee these two conditions by the setting of the inlet boundary alone, thus they are guaranteed by both the inlet and open boundary settings:

a. Quasi-neutrality $n_{i0} = n_{e0}$ and current-free condition $j_{i0} = j_{e0}$ is forced at the inlet boundary;
b. Return those electrons crossing open boundaries but with relatively lower energy based on the global current-free condition at each time step.

Therefore, at the inlet boundary, the number of electrons and ions injected per time step should be equal, and the axial component of electron velocity at the inlet v_{ez0} should include both the thermal velocity v_{ez} and a drifting velocity equal to the one of ions,

$$v_{ez0} = v_{ez} + v_0 \tag{5}$$

III. Results and discussion

A. Reproduction and analysis of the detachment cone

The simulation is conducted to reproduce the phenomenon and the inlet parameters are set to resemble the plume of our MPDT at JLPP. The inlet electron and ion temperature is set respectively as 10 eV and 0.1 eV to include the thermal energy of both species. As presented by Merino et al.[38], the normalized ion cyclone frequency $\widehat{\Omega}_{i0} = {R_{p0}\Omega_{i0}}/{v_0}$ is also employed to evaluate the relative magnetization degree. And as we have shrunken the simulation domain, the magnitude of the applied magnetic field should be modified to keep the same relative magnetization degree as in our former experiment. Therefore, the magnitude of inductive magnetic strength at the plasma inlet is $\mathrm{B}_0 = 0.85T$.

The simulation process takes about 20,000 time steps to converge, and the simulation results are presented in Figure 5. As can be seen from Figure 5 (a), the detachment cone has been reproduced in the density contour, and the structure is outside the most divergent magnetic line (MDML), which resembles the density structure in Figure 2 very well. Then the PIC model can be used to investigate the mechanism of this phenomenon.

Since the density structure lies outside the MDML, a question arises that how the plasma can be transported there. An obvious answer would be that the ions are not magnetized enough to keep their trajectories along the magnetic lines. In fact, the Larmor radius of ions in the plasma inlet normalized by the characteristic length of the system can be calculated as,

$$\widehat{r_{Li}} = \frac{m_i v_{thi}}{B_0 q_i R_{p0}} = \frac{\sqrt{k_B T_i m_i}}{B_0 q_i R_{p0}} = 0.42 \tag{6}$$

in which the characteristic length of the system is the inlet radius $R_{p0} = 10\lambda_0$.

From this criterion, the normalized Larmor radius of ions cannot satisfy $\widehat{r_{Li}} \ll 1$, so the ions are not magnetized, hence the ions will not follow the magnetic lines exactly and expand out of the MDML. To maintain quasi-neutrality electrons will also expand out of the MDML.

From energy perspective, the thermal energy drives the ions to expand downstream. The ion temperature distribution is shown in Figure 5 (b), the ion temperature mostly vanishes near the plasma inlet especially in the axial direction, which indicates a fast conversion from thermal energy to kinetic energy of ions near the plasma inlet. Hence in the early stage of expansion, the population of ions are accelerated towards two perpendicular directions.

In Figure 5 (c), the ion streamlines are illustrated as red solid lines with arrows and the electric potential distribution is shown in contour. Judging from the streamlines and the ion density distribution, most of ions are accelerated axially and constitute the beam on the thruster axis, while some of them are accelerated radially. The axially and radially accelerated plasma constitute the main beam and the side beam respectively. Note that our model is planar, the side beam will become a cone-shaped structure in 3D or 2D-axisymetic geometries, the "hollow" area between the cone-shaped side beam and the central main beam is the detachment cone.

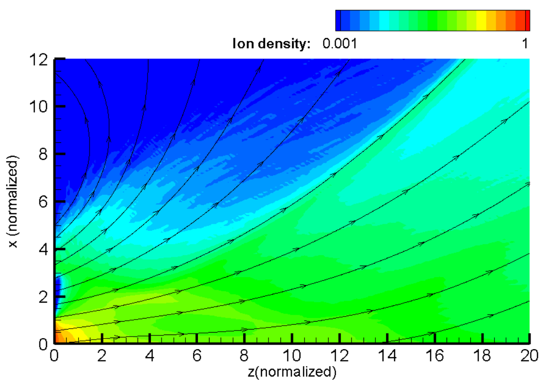

(a) Ion density contour

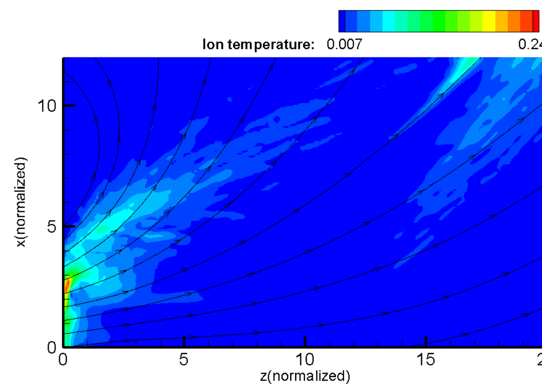

(b) Ion temperature contour

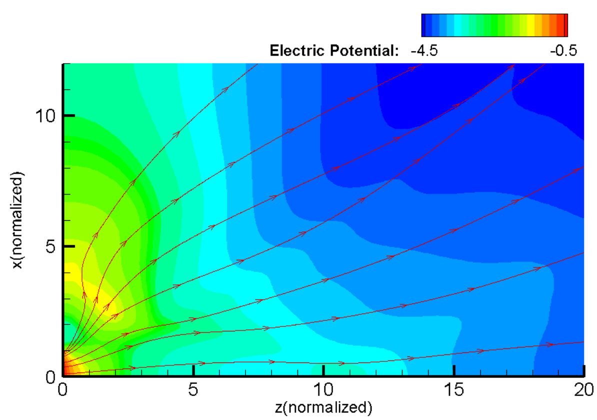

(c) Electric potential contour

Figure 5 Plasma parameters simulated in the reproduction case ($T_e = 10$ eV, $T_i = 0.1$ eV, $B_0 = 0.85$ T), (a) ion density distribution, (b) Ion temperature distribution, (c) Electric potential distribution, all the parameters have been normalized. The black streamlines is the magnetic lines and the red ones in (c) is the ion trajectories.

Another question arises that how the non-magnetized ions are constrained in the radial downstream as a cone-shape area rather than a fan-shaped area. The electric force is the only option since Lorentz force cannot provide the constraint. The electric potential distribution is shown in Figure 5 (c), there is a high potential area above the plasma inlet. This high potential works like a potential barrier to reduce the x-velocity of ions, thus bend the streamlines downstream. That is the reason why the side beam is cone-shaped rather than fan-shaped.

The generation mechanism of the potential barrier is not analyzed in detail, however it is believed that different magnetization degree between ions and electrons are the main reason for the potential barrier. The normalized Larmor radius of electrons indicates that the electrons are magnetized well,

$$\widehat{r_{Le}} = \frac{m_e v_{the}}{B_0 q_e R_{p0}} = \frac{\sqrt{k_B T_e m_e}}{B_0 q_e R_{p0}} = 0.098 \ll 1, \quad (7)$$

the non-magnetized ions can expand in the $B_\perp$ direction with little constraint from the Lorenz forces, while the strongly magnetized electrons cannot. In order to maintain quasi-neutrally, a local high potential area is induced to hold the ions and electrons together. Similar potential structures are reported in literatures[36,42,43], but they may have differences and require further investigations which are not within the scope of this paper.

B. Parametric study

It can be summarized from the last section that the detachment is closely related to ion thermal energy and the magnetic field, hence a parametric study on the influence of ion temperature and magnetic inductive strength need to be conducted using the Particle-in-Cell code.

First, the ion temperature is kept the same (0.1eV), and the magnetic inductive strength at the plasma inlet is set as 0.4T, 1.7T and 2.55T respectively, the rest of the simulation conditions are the same as the reproduction case. The ion density distribution of the four cases with different B_0 is presented in Figure 6. As is seen from the figure, the detachment cone is more obvious when reduces B_0 to 0.4T, the side beam expand further deep into the radial downstream and even flows out of the left boundary, which is certainly harmful for the propulsive performances and may have plume pollution problems with the spacecraft in practical cases. However, the detachment cone is severely suppressed in the cases of 1.7T and 2.55T due to more ion magnetization and the plume divergence angle is much smaller than that of lower B_0 cases, which will result in better nozzle efficiency. This is the first mechanism for suppressing the detachment cone – ion magnetization.

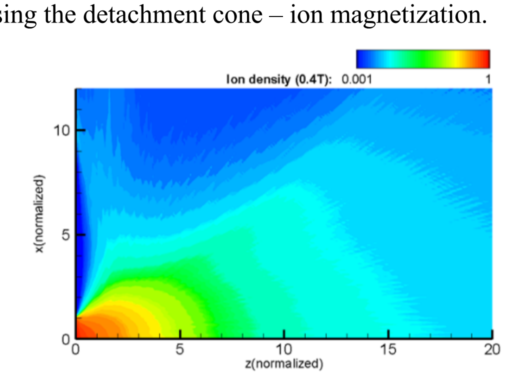

(a) $B_0 = 0.4T$

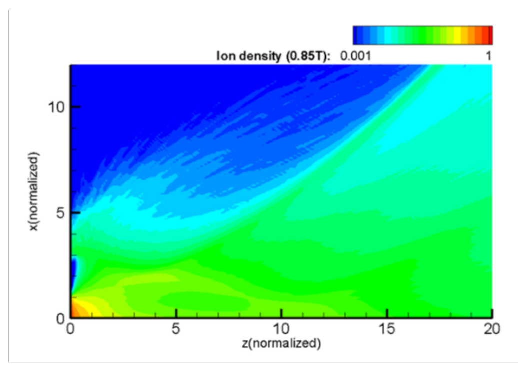

(b) $B_0 = 0.85T$

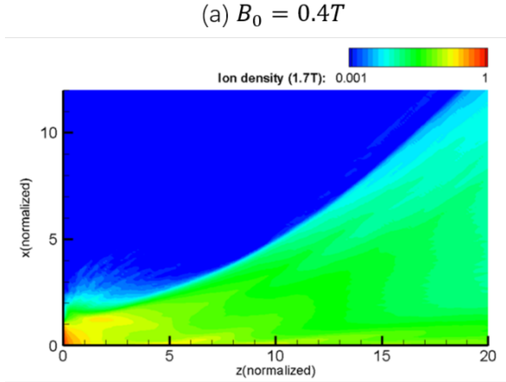

(c) $B_0 = 1.7T$

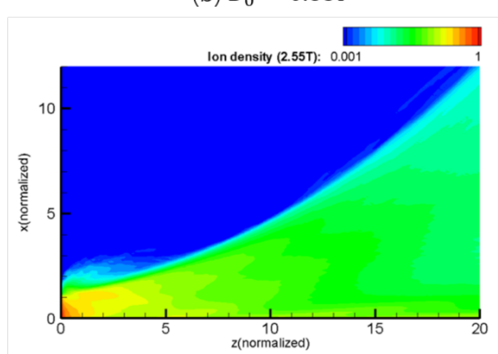

(d) $B_0 = 2.55T$

Figure 6 Ion density distribution VS. magnetic inductive strength B_0

The radial profile of electric potential at $\hat{z} = 1$ for simulation cases with different B_0 is plotted in **Figure 7**, there is no sign of potential barrier in the 0.4T case, as B_0 increases, the potential barrier appears, the maxima of the potential barrier grows higher as B_0 increases. The reason for this trend is that when B_0 is lower than 0.4T, electrons are less magnetized, the magnetization difference between ions and electrons is decreased, thus the potential barrier disappears. When B_0 increases, the magnetization of electrons strengthens, while the ions are more insensitive to the B_0 increasement, which promotes the magnetization difference, hence the potential barrier becomes more profound. However, as B_0 grows over 1.7T, the magnitude of the potential barrier seems saturates, as the ions are becoming more magnetized hence the requirement to confine the ions for the potential barrier is lowered. This trend explains another mechanism that suppress the detachment cone – the potential barrier, which has a competing relationship with ion magnetization. Therefore, an optimized magnetic inductive strength exists.

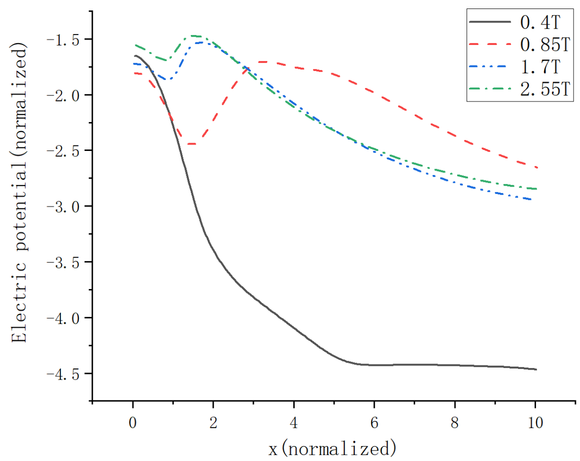

Figure 7 Radial electric potential profile at $\hat{z} = 1$

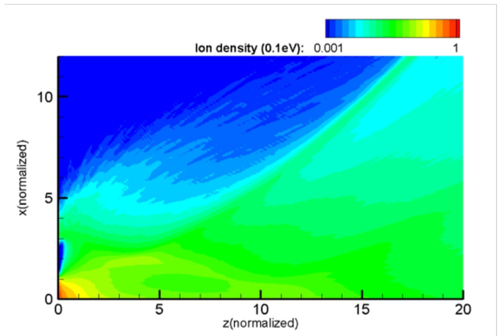

(a) $T_i = 0.1eV$

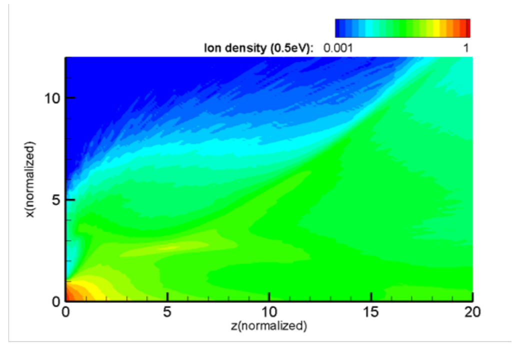

(b) $T_i = 0.5eV$

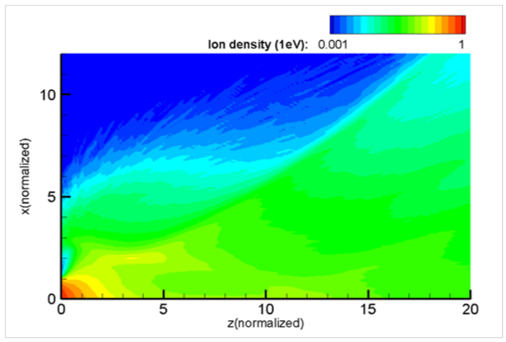

(c) $T_i = 1eV$

Figure 8 Ion density distribution VS. ion temperature

The second parameter study focuses on the influence of ion temperature, as the ion thermal energy is the internal drive for the detachment cone. The magnetic inductive strength at the plasma inlet $B_0 = 0.85T$ is kept constant, and the ion temperature is set as 0.5 eV, 1.0eV, the rest of the parameters are the same as the reproduction case. The simulated results of ion density distribution for the three cases are shown in Figure 8.

As the ion temperature increases, the size of the side beam grows larger and contact directly with the main beam, which can be explained by the increased thermal energy of ions, hence the detachment cone disappears. However, when T_i increased from 0.5eV to 1.0eV, the side beam does not grow larger which is unexpected and needs further investigations.

IV. Conclusion

This paper employs a particle-in-cell model to reproduce and investigate a phenomenon called detachment cone observed in a MPDT experiment at JLPP. The phenomenon is successfully reproduced, and some parametric studies are conducted to investigate the influence of magnetic inductive strength B_0 and the ion temperature T_i on the detachment cone.

The detachment cone is a hollow region between the central main beam and the side beam, and it's caused by the thermalized ions which are insufficiently magnetized expanding and detaching from the magnetic nozzle in the outside direction. These detached ions form a side beam and significantly increase the divergent angle, hence undermines the propulsive performance of the electric thruster. According to the parametric studies, the detachment cone will be greatly suppressed as the magnetic inductive strength strengthens, behind which there are two competing mechanisms – ion magnetization and the potential barrier, hence an optimized B_0 exists and should be determined to suppress the phenomenon. As the ion temperature grow larger, the side beam will be larger, hence hindering the propulsive performances. Therefore, another effective method to suppress the phenomenon is to deposite more power into electrons than ions in the plasma source. Also, a phenomenon named potential barrier is discovered in the simulation and may play an important role in the plasma acceleration. The optimization of B_0 and mechanisms of the potential barrier deserve further investigations in the future.

Acknowledgements

This work was supported by the National Natural Science Foundation of China (Grant No. 11872093). And the authors would like to thank Master candidate Yifeng Fu, Doctor Candidates Shuai Cao and Ruojian Pan for some useful discussions.

References

[1] Y. Arakawa and A. Sasoh, Journal of Propulsion and Power **8**, 98 (1992).
[2] C. Charles and R. Boswell, Applied Physics Letters **82**, 1356 (2003).
[3] A.V. Arefiev and B.N. Breizman, Physics of Plasmas **11**, 2942 (2004).
[4] M. Keidar, in *53rd AIAA Aerospace Sciences Meeting* (American Institute of Aeronautics and Astronautics, n.d.).
[5] K.F. Schoenberg, R.A. Gerwin, R.W. Moses Jr, J.T. Scheuer, and H.P. Wagner, Physics of Plasmas **5**, 2090 (1998).
[6] C. Charles, R.W. Boswell, W. Cox, R. Laine, and P. MacLellan, Applied Physics Letters **93**, 201501 (2008).
[7] M. Merino and E. Ahedo, Plasma Sources Science and Technology (2017).
[8] B. Lin and J. Sheehan, in (American Institute of Aeronautics and Astronautics, 2018).
[9] S.A. Andersen, Physics of Fluids **12**, 557 (1969).
[10] K. Kuriki and O. Okada, The Physics of Fluids **13**, 2262 (1970).
[11] T. YORK, B. JACOBY, and P. Mikellides, Journal of Propulsion and Power **8**, 1023 (1992).
[12] I. Masaaki, A. Akira, H. Kunihiko, T. Hiroyuki, and Y. TSuyoshi, 9 (2002).
[13] G.R. Seikel and E.L. Walker, (1971).
[14] H.G. Kosmarbl, 31 (n.d.).
[15] D.L. Chubb, AIAA Journal **10**, 113 (1972).
[16] P.G. Mikellides, P.J. Turchi, and N.F. Roderick, Journal of Propulsion and Power **16**, 887 (2000).
[17] M. Li, H.-B. Tang, J.-X. Ren, and T.M. York, Phys. Plasmas **20**, (2013).
[18] J. Cheng, H.-B. Tang, and T.M. York, Phys. Plasmas **21**, (2014).
[19] A.V. Arefiev and B.N. Breizman, Physics of Plasmas **15**, 042109 (2008).
[20] J.P. Sheehan, B.W. Longmier, E.A. Bering, C.S. Olsen, J.P. Squire, M.G. Ballenger, M.D. Carter, L.D. Cassady, F.R. Chang Díaz, T.W. Glover, and A.V. Ilin, Plasma Sources Science and Technology **23**, 045014 (2014).
[21] R.W. Moses, R.A. Gerwin, and K.F. Schoenberg, in (AIP, 1992), pp. 1293–1303.
[22] E.B. Hooper, Journal of Propulsion and Power **9**, 757 (1993).
[23] A.V. Arefiev and B.N. Breizman, Physics of Plasmas **12**, 043504 (2005).
[24] D. Kaufman, D. Goodwin, and J. Sercel, in (American Institute of Aeronautics and Astronautics, 1993).
[25] J.M. Little and E.Y. Choueiri, in *Proceedings of 47th Joint Propulsion Conference, San Diego, CA, AIAA* (2011).
[26] E. Ahedo and M. Merino, Physics of Plasmas **18**, 053504 (2011).
[27] A.V. Ilin, F.R. Chang-Diaz, J.P. Squire, A.G. Tarditi, B.N. Breizman, and M.D. Carter, AIAA Paper **346**, (2002).
[28] R. Winglee, T. Ziemba, L. Giersch, J. Prager, J. Carscadden, and B.R. Roberson, Physics of Plasmas **14**, 063501 (2007).
[29] M. Merino and E. Ahedo, Plasma Sources Science and Technology **25**, 045012 (2016).
[30] M. Merino and E. Ahedo, in *Proceedings of 47th Joint Propulsion Conference, San Diego, CA (American Institute of Aeronautics and Astronautics, Washington DC, 2011), AIAA Paper* (2011).
[31] S.A. Cohen and M.A. Paluszek, Launchspace **3**, 46 (1998).
[32] Y. Xu and H. Tang, in *Proc. Int. Electric Propulsion Conf* (2013).
[33] C. Charles, Applied Physics Letters **96**, 051502 (2010).
[34] K. Takahashi, C. Charles, R. Boswell, W. Cox, and R. Hatakeyama, Appl. Phys. Lett. **94**, 191503 (2009).
[35] S.K. Saha, S. Chowdhury, M.S. Janaki, A. Ghosh, A.K. Hui, and S. Raychaudhuri, Physics of Plasmas **21**, 043502 (2014).
[36] N. Singh, S. Rao, and P. Ranganath, Physics of Plasmas **20**, 032111 (2013).
[37] S. Rao and N. Singh, Physics of Plasmas **19**, 093507 (2012).
[38] E. Ahedo and M. Merino, Physics of Plasmas **19**, 083501 (2012).
[39] K.L. Cartwright, J.P. Verboncoeur, and C.K. Birdsall, Journal of Computational Physics **162**, 483 (2000).
[40] M. Li, M. Merino, E. Ahedo, J. Ren, and H. Tang, in *Proc. Int. Electric Propulsion Conf* (2017).
[41] M. Li, M. Merino, E. Ahedo, and H. Tang, Plasma Sources Sci. Technol. (2019).
[42] S.K. Saha, S. Raychaudhuri, S. Chowdhury, M.S. Janaki, and A.K. Hui, Physics of Plasmas **19**, 092502 (2012).
[43] J.M. Little, Performance Scaling of Magnetic Nozzles for Electric Propulsion, n.d.